Phytochemistry 180 (2020) 112527

Contents lists available at ScienceDirect

Phytochemistry

journal homepage: www.elsevier.com/locate/phytochem

Structural and functional features of a class VI chitinase from cashew (*Anacardium occidentale* L.) with antifungal properties

Simone T. Oliveira [a], Mayara I.G. Azevedo [a], Rodrigo M.S. Cunha [b], Christiana F.B. Silva [c], Celli R. Muniz [c], José E. Monteiro-Júnior [d], Rômulo F. Carneiro [e], Celso S. Nagano [e], Matheus S. Girão [a], Cleverson D.T. Freitas [a], Thalles B. Grangeiro [d,*]

[a] Departamento de Bioquímica e Biologia Molecular, Universidade Federal do Ceará, Fortaleza, Ceará, Brazil
[b] Centro de Ciências Agrárias e Biológicas, Universidade do Vale do Acaraú, Sobral, Ceará, Brazil
[c] Embrapa Agroindústria Tropical, Fortaleza, Ceará, Brazil
[d] Laboratório de Genética Molecular, Departamento de Biologia, Universidade Federal do Ceará, Fortaleza, Ceará, Brazil
[e] Departamento de Engenharia de Pesca, Universidade Federal do Ceará, Fortaleza, Ceará, Brazil

ARTICLE INFO

Keywords:
Anacardium occidentale
Anacardiaceae
Cashew
Biochemical characterization
Protein
Chitinase
AoChi

ABSTRACT

A partial cDNA sequence from *Anacardium occidentale* CCP 76 was obtained, encoding a GH19 chitinase (AoChi) belonging to class VI. AoChi exhibits distinct structural features in relation to previously characterized plant GH19 chitinases from classes I, II, IV and VII. For example, a conserved Glu residue at the catalytic center of typical GH19 chitinases, which acts as the proton donor during catalysis, is replaced by a Lys residue in AoChi. To verify if AoChi is a genuine chitinase or is a chitinase-like protein that has lost its ability to degrade chitin and inhibit the growth of fungal pathogens, the recombinant protein was expressed in *Pichia pastoris*, purified and biochemically characterized. Purified AoChi (45 kDa apparent molecular mass) was able to degrade colloidal chitin, with optimum activity at pH 6.0 and at temperatures from 30 °C to 50 °C. AoChi activity was completely lost when the protein was heated at 70 °C for 1 h or incubated at pH values of 2.0 or 10.0. Several cation ions (Al^{3+}, Cd^{2+}, Ca^{2+}, Pb^{2+}, Cu^{2+}, Fe^{3+}, Mn^{2+}, Rb^{+}, Zn^{2+} and Hg^{2+}), chelating (EDTA) and reducing agents (DTT, β-mercaptoethanol) and the denaturant SDS, drastically reduced AoChi enzymatic activity. AoChi chitinase activity fitted the classical Michaelis-Menten kinetics, although turnover number and catalytic efficiency were much lower in comparison to typical GH19 plant chitinases. Moreover, AoChi inhibited *in vitro* the mycelial growth of *Lasiodiplodia theobromae*, causing several alterations in hyphae morphology. Molecular docking of a chito-oligosaccharide in the substrate-binding cleft of AoChi revealed that the Lys residue (theoretical pK_a = 6.01) that replaces the catalytic Glu could act as the proton donor during catalysis.

1. Introduction

Chitinases (EC 3.2.1.14) are glycoside hydrolases (GHs) that cleave the β-(1 → 4)-glycosidic linkages of chitin [(1 → 4)-2-acetamido-2-deoxy-β-D-glucan], a linear homopolysaccharide constituted by units of *N*-acetyl-β-D-glucosamine [β-D-(acetylamino)-2-deoxy-glucopyranose; GlcNAc]. Chitin is the second most abundant biopolymer on earth, the first one being cellulose. This polysaccharide is found in a wide range of organisms, including species of Fungi, Arthropoda, Mollusca and Nematoda (Crini, 2019). Chitin is an important structural component of the cell wall of most Fungi and the extracellular matrices of Arthropoda exoskeletons (Gow et al., 2017; Liu et al., 2019).

Chitinases are widespread in nature, occurring in diverse organisms belonging to Archaea, Bacteria and Eukaryota. Based on similarities in their primary and three-dimensional structures, most known chitinases have been classified in the families GH18 and GH19, according to the rules of the Carbohydrate-Active Enzymes (CAZy) database (Lombard et al., 2014). GH18 and GH19 chitinases have different three-dimensional structures and employ distinct catalytic mechanisms. GH18 enzymes adopt a $(\beta/\alpha)_8$ barrel fold and perform catalysis using a double displacement retaining mechanism (Terwisscha van Scheltinga et al., 1995). Conversely, GH19 proteins adopt a lysozyme-like fold, catalyzing the cleavage of chitin using a single displacement inverting mechanism (Brameld and Goddard, 1998; Hart et al., 1995).

* Corresponding author.
E-mail address: thalles@ufc.br (T.B. Grangeiro).

https://doi.org/10.1016/j.phytochem.2020.112527
Received 30 January 2020; Received in revised form 25 April 2020; Accepted 21 September 2020
Available online 29 September 2020
0031-9422/

In plants, chitinases are encoded by large gene families, distributed in different chromosomes and usually encoding both GH18 and GH19 enzymes (Mir et al., 2020). Plant chitinases are defense proteins that act on chitin chains of fungal cell walls, restricting the growth and spread of pathogenic fungi. Besides this direct suppressive effect on fungal pathogens, the hydrolysis of fungal chitin chains promoted by host chitinases releases chito-oligosaccharides that are recognized by lysin-motif containing plant receptors, triggering host immune responses (Volk et al., 2019). Due to the association of several plant chitinases with resistance reactions to pathogens, many of these molecules have been classified as pathogenesis-related proteins (PR-proteins), constituting the families PR-3, PR-4, PR-8 and PR-11 (van Loon et al., 2006).

Independent of their involvement in defense mechanisms, GH19 chitinases from plants have been grouped in 5 different classes (I, II, IV, VI and VII), according to domain architecture and sequence identity. Class I members have a primary structure similar to tobacco (*Nicotiana tabacum*) chitinases CHN50 and CHN48, which have a hevein-like, chitin-binding domain (ChBD) at the N-terminal region, a linker region rich in Thr, Pro and Gly residues, a GH19 catalytic domain and a C-terminal extension (CTE) (Shinshi et al., 1990). Class II chitinases contain a catalytic domain (CatD) that shares high sequence identity with the CatD of class I members, but do not have the ChBD at the N-terminal region (Shinshi et al., 1990). Class IV chitinases, as first identified in common bean (*Phaseolus vulgaris*), are related to class I, but are shorter due to one deletion in the ChBD and 3 deletions in the CatD, corresponding to loops II, IV and V, according to the nomenclature of Taira et al. (2011). Class IV members also do not have the CTE or C-terminal loop (Collinge et al., 1993; Margis-Pinheiro et al., 1991). Class VII chitinases are related to class IV, exhibiting the same 3 deletions in the CatD and the absence of a CTE, but the hevein-like, N-terminal ChBD is missing (Gonzalez et al., 2015; Kolosova et al., 2014; Neuhaus, 1999). Chitinases from class VI *sensu* Tyler et al. (2010) have similar sizes when compared to class I chitinases (*ca.* 295–305 amino acid residues), but the N-terminal region in front of the CatD has little similarity with the hevein-like domain, and they are grouped in a distinct clade. The better studied members of this class are those encoded by genes *AtCTL1* and *AtCTL2* from *Arabidopsis thaliana* (Hossain et al., 2010; Zhong et al., 2002). In AtCTL1 and AtCTL2, as well as in their homologous proteins from cotton (*Gossypium hirsutum*), GhCTL1 and GhCTL2 (Zhang et al., 2004), a conserved Glu residue, that acts as the proton donor during catalysis by GH19 chitinases, is replaced by a Lys residue. Due to this mutation, AtCTL1, AtCTL2 and related molecules have been classified as chitinase-like proteins (CLPs), presumably lacking hydrolytic activity towards chitin. Contrary to chitinases that participate in defense mechanisms against pathogens, AtCTL1 and other class VI CLPs seem to play important roles in normal plant growth and development processes, like lignin deposition, cellulose synthesis, and determination of root and shoot architectures (Kesari et al., 2015).

Cashew (*Anacardium occidentale* L.) is an evergreen tree from the family Anacardiaceae, which includes mango tree (*Mangifera indica*) and pistachio (*Pistacia vera*), for example. The species *A. occidentale* is native to the Caribbean Islands and Central and northern South America, including the Northeast region of Brazil (Johnson, 1973). A heat-labile chitinolytic activity has been reported in cashew gum exudates, and a probable role for the uncharacterized chitinases responsible for this enzymatic activity as a biochemical defense against pathogens or insect pests was speculated (Rita Marques and Xavier-Filho, 1991). However, to the best of our knowledge, further details about structural and biochemical features of cashew chitinases have not been reported yet. In this work, a class VI chitinase from cashew was expressed in *Pichia pastoris*, purified and biochemically characterized. Despite its distinct structural features, including the substitution of the catalytic Glu for a Lys residue, the recombinant protein showed hydrolytic activity on colloidal chitin and inhibited *in vitro* the mycelial growth of *Lasiodiplodia theobromae* (Pat.) Griffon & Maubl., a plant pathogenic fungus with a wide host range.

2. Results and discussion

2.1. Structural and functional features of a GH19 chitinase encoded by a partial cDNA from Anacardium occidentale CCP 76

A partial cDNA sequence encoding a GH19 chitinase was obtained from the dwarf clone CCP 76 of *Anacardium occidentale* (Figs. S2 and S3). This cDNA sequence encodes a protein with 322 amino acid residues, containing a signal peptide at the N-terminal region (residues 1–23; Fig. S4) and a chitinase_GH19 domain (CDD domain model accession number: cd00325; residues 64–306), which is a member of the lysozyme-like superfamily (CDD accession number: cl00222) (Fig. 1A). The searches against the databases CDD and SMART showed that, besides the catalytic domain, cashew GH19 chitinase does not have any other recognizable accessory domain (Fig. S5), like the chitin-binding type-1 domain (ChtBD1). ChtBD1, which is also known as hevein-like domain, is found at the N-terminal region of plant chitinases from classes I and IV. Plant GH19 chitinases that do not have a typical chitin-binding domain are classified in classes II, VI or VII, according to the presence/absence of certain loop regions in the catalytic domain and the level of sequence identity among them. Therefore, to determine with confidence to which class the cashew chitinase (AoChi) belongs to, its amino acid sequence was aligned to primary structures of representative plant GH19 chitinases from classes I, II, IV, VI and VII. Inspection of the multiple alignment clearly evidenced the closer relationship of cashew chitinase with members of class VI *sensu* Tyler et al. (2010), such as AtCTL1 and AtCTL2 (Fig. S6). Indeed, sequence identity between AoChi and AtCTL1 and AtCTL2 was *ca.* 73% and 79%, respectively. On the other hand, when AoChi was compared to representative chitinases from classes I, II, IV and VII, sequence identity percentages varied from 21.7% to 33.4% (Table S1). To strength this assumption, the primary structure of AoChi was aligned with diverse members of each class of GH19 plant chitinases (Table S2 and Fig. S7) and a phylogenetic analysis was performed. As depicted in Fig. 2, five supported clades were recovered, four of them containing sequences belonging to a single chitinase class, II, IV, VI and VII, whereas a fifth clade contained sequences from classes I and II. These results agree with previous works, that have suggested that chitinases from classes I and II have originated from a common ancestral protein (Gonzalez et al., 2015; Tyler et al., 2010). AoChi sequence was recovered within one the five supported clades, which grouped all class VI chitinases. Therefore, cashew chitinase was designated as a new member of class VI chitinases.

The alignment of the GH19 CatD of AoChi with known GH19 structures of plant chitinases revealed some important structural differences in relation to genuine chitinases (Fig. 3). For example, GH19 chitinases are inverting enzymes, which catalyze the hydrolysis of chitin β-(1 → 4)-linkages using a single displacement mechanism, with inversion of the stereochemistry of the anomeric carbon (Iseli et al., 1996; Fukamizo et al., 1995). The catalytic center of GH19 chitinases is characterized by a conserved pattern of 3 residues, Glu-X_n-Glu-X_n-Ser/Thr, in which the first Glu acts as the catalytic acid and the second Glu is the general catalytic base. The catalytic mechanism of inverting GHs involves a single step: the carboxylate group of the first Glu donates a proton to the O atom of the scissile glycosidic bond, and simultaneously, the carboxylate group of the second Glu, with the contribution of the polar side chain of a Ser or Thr residue, assists the nucleophilic attack of a water molecule on the anomeric carbon of the leaving group, thus completing the hydrolysis of the glycosidic bond (Mayes et al., 2016). Notably, in cashew chitinase, the residues putatively involved in catalysis were identified as Lys^{128}, Glu^{150} and Tyr^{183} (Fig. 3). The same residues are also found in other class VI chitinases (Fig. 1B, S6 and S7). Moreover, the GH19 domain of plant chitinases is stabilized by 3 disulfide bonds (Landim et al., 2017), involving 6 conserved Cys residues (Cys^1 to Cys^6), as shown in the multiple sequence alignment of representative plant chitinases from classes I, II, IV, VI and VII (Figs. S6 and S7). However, in the primary structure of AoChi

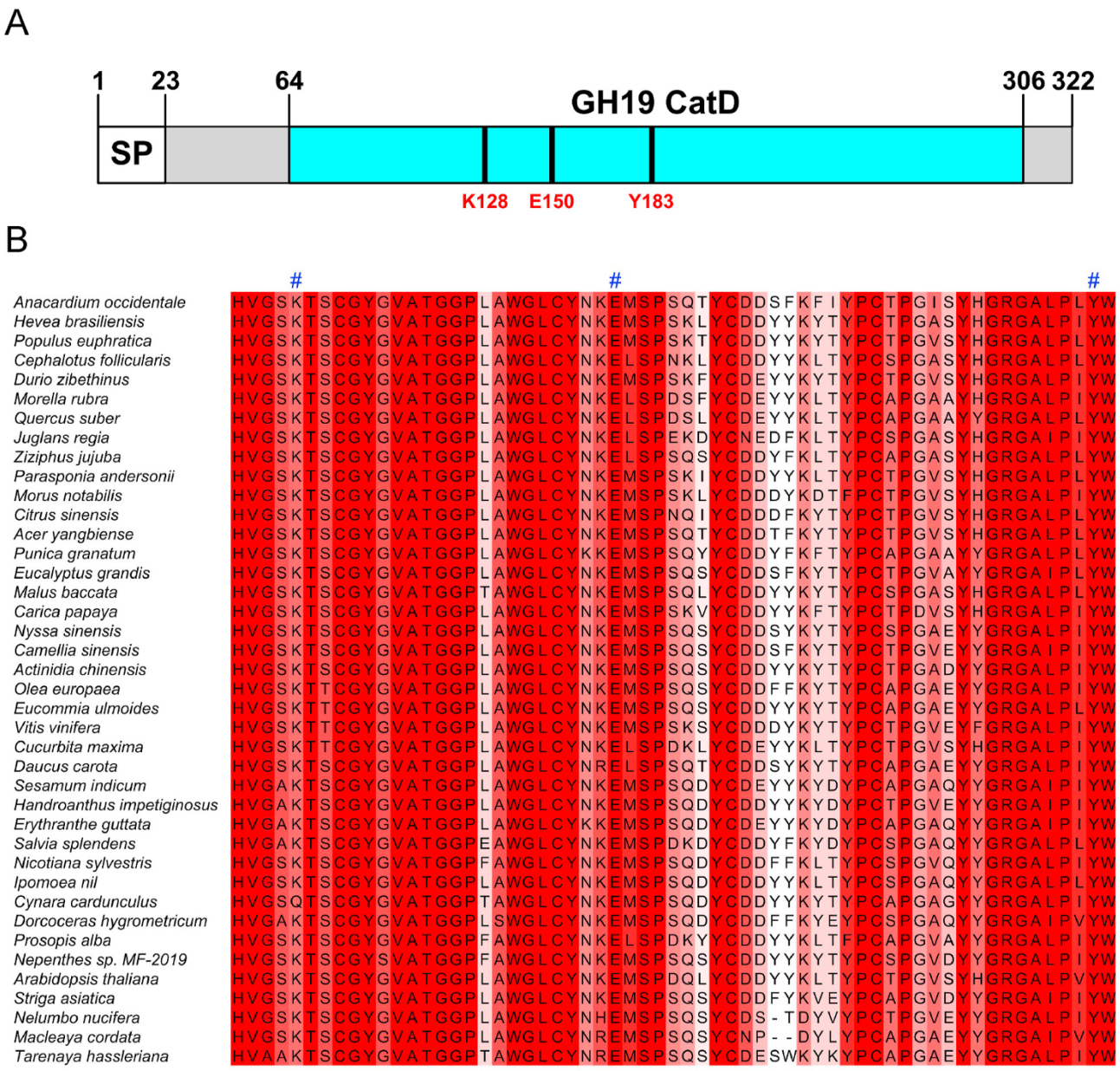

Fig. 1. Domain architecture of *Anacardium occidentale* chitinase (AoChi). (A) Graphical representation of AoChi domains (SP: signal peptide; GH19 CatD: GH19 catalytic domain). The catalytic residues of AoChi, Lys(K)^{128}, Glu(E)^{150} and Tyr(Y)^{183}, are highlighted. (B) Alignment of a stretch of 61 residues from the primary structure of AoChi (from His^{124} to Trp^{184}), which contains the 3 catalytic residues, with corresponding segments from homologous proteins belonging to plant species from different families and orders (Table S5). Alignment columns are colored according to the ALSCRIPT Calcons convention, as implemented in ALINE (Bond and Schüttelkopf, 2009), using a predefined color scheme, which reflects the conservation of amino acid properties in each column (dark red: identical residues; white: dissimilar residues). (For interpretation of the references to color in this figure legend, the reader is referred to the Web version of this article.)

(Fig. 3), Cys^{1} (located in loop I) is replaced by an Ala residue (Ala^{82}), whereas a new Cys residue emerged at another site (Cys^{131}), replacing a Gly residue (located in loop II) that is conserved in chitinases from classes I and II or absent in chitinases belonging to classes IV and VII (Figs. S6 and S7). These two mutations involving conserved Cys and Gly residues were also found in all class VI chitinases analyzed (Fig. S7). Another structural feature of AoChi is the insertion of a 5-residues peptide (^{294}GREEA^{298}) near the C-terminal end (labeled as loop VI in Fig. 3), which was not found in chitinases from classes I, II, IV and VII, but is conserved in members of class VI (Fig. S7).

To verify if the cashew GH19 protein is a true chitinase, able to hydrolyze chitin and inhibit the growth of phytopathogenic fungi, or is a chitinase-like protein (CLP), which has lost its enzymatic activity due to these mutations in the catalytic center, the protein was produced in *P. pastoris*, purified and partially characterized.

2.2. Biochemical characterization of the recombinant class VI chitinase from A. occidentale

When cultivated in the presence of methanol, clones of *P. pastoris* KM71H that were transformed with a recombinant expression cassette containing the DNA sequence encoding the mature form of AoChi, secreted into the culture medium a major protein band with an apparent molecular mass of *ca.* 45 kDa (Fig. S10). The recombinant protein was purified by affinity chromatography on a resin with immobilized Ni^{2+} ions (Fig. S11), and when subjected to SDS-PAGE, the recombinant product showed an acceptable degree of purity (Fig. 4A). The identity of this band as the recombinant cashew chitinase was confirmed by tandem

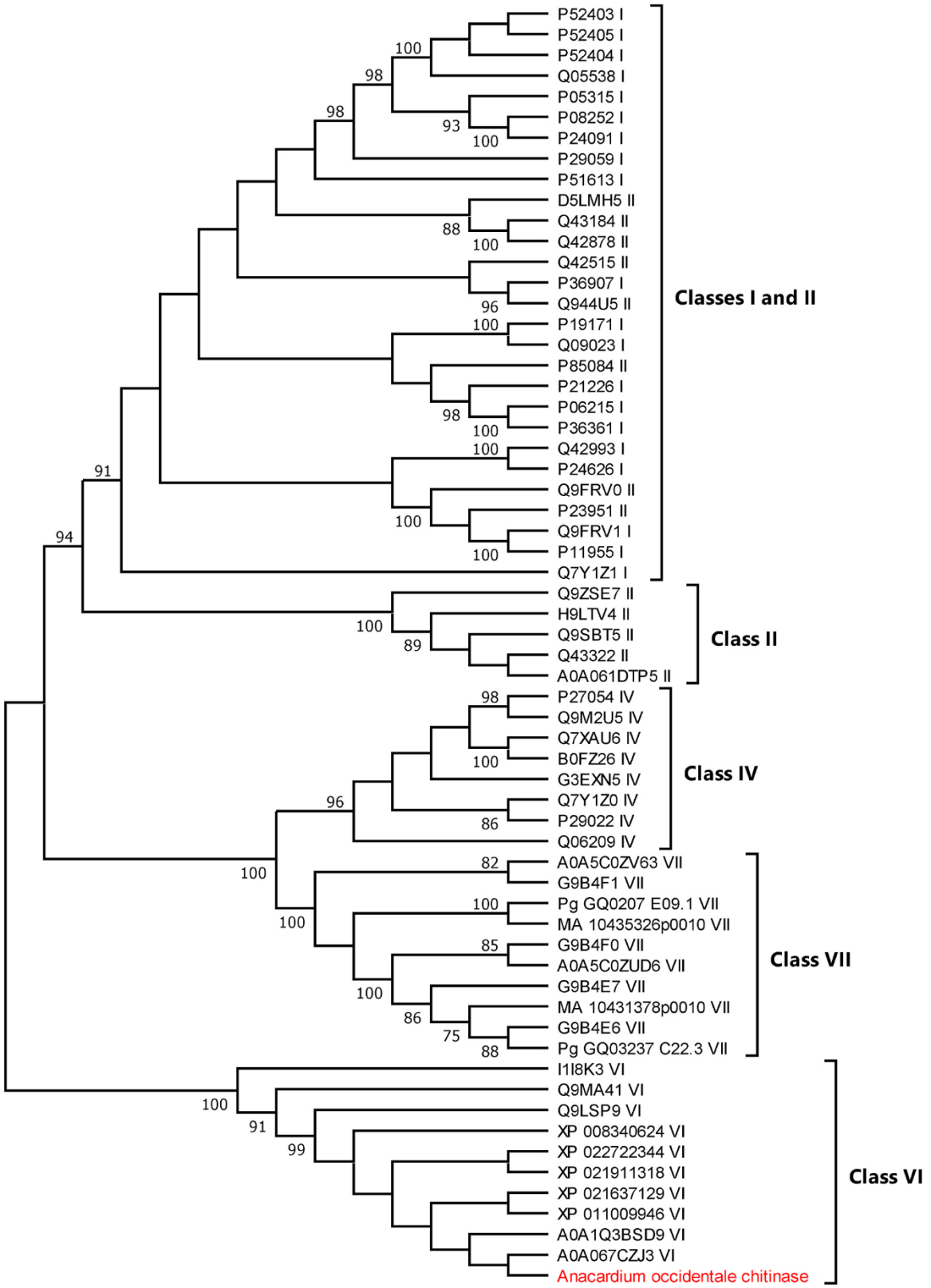

Fig. 2. Maximum likelihood (ML) tree showing the phylogenetic relationship of *Anacardium occidentale* chitinase with representative plant chitinases from classes I, II, IV, VI and VII. The evolutionary history of the sequences was inferred by using the ML method and Whelan and Goldman + Freq. model (Whelan and Goldman, 2001). The tree with the highest log likelihood (−12837.58) is shown. A discrete Gamma distribution was used to model evolutionary rate differences among sites (5 categories (+G, parameter = 1.5328)). The rate variation model allowed for some sites to be evolutionarily invariable ([+I], 3.91% sites). The percentage of trees in which the associated sequences clustered together, as determined by the bootstrap test (100 replicates), is shown next to the branches. This analysis involved 62 amino acid sequences, and the final dataset contained a total of 371 positions (Table S2 and Fig. S7). Evolutionary analyses were conducted in MEGA X (Kumar et al., 2018).

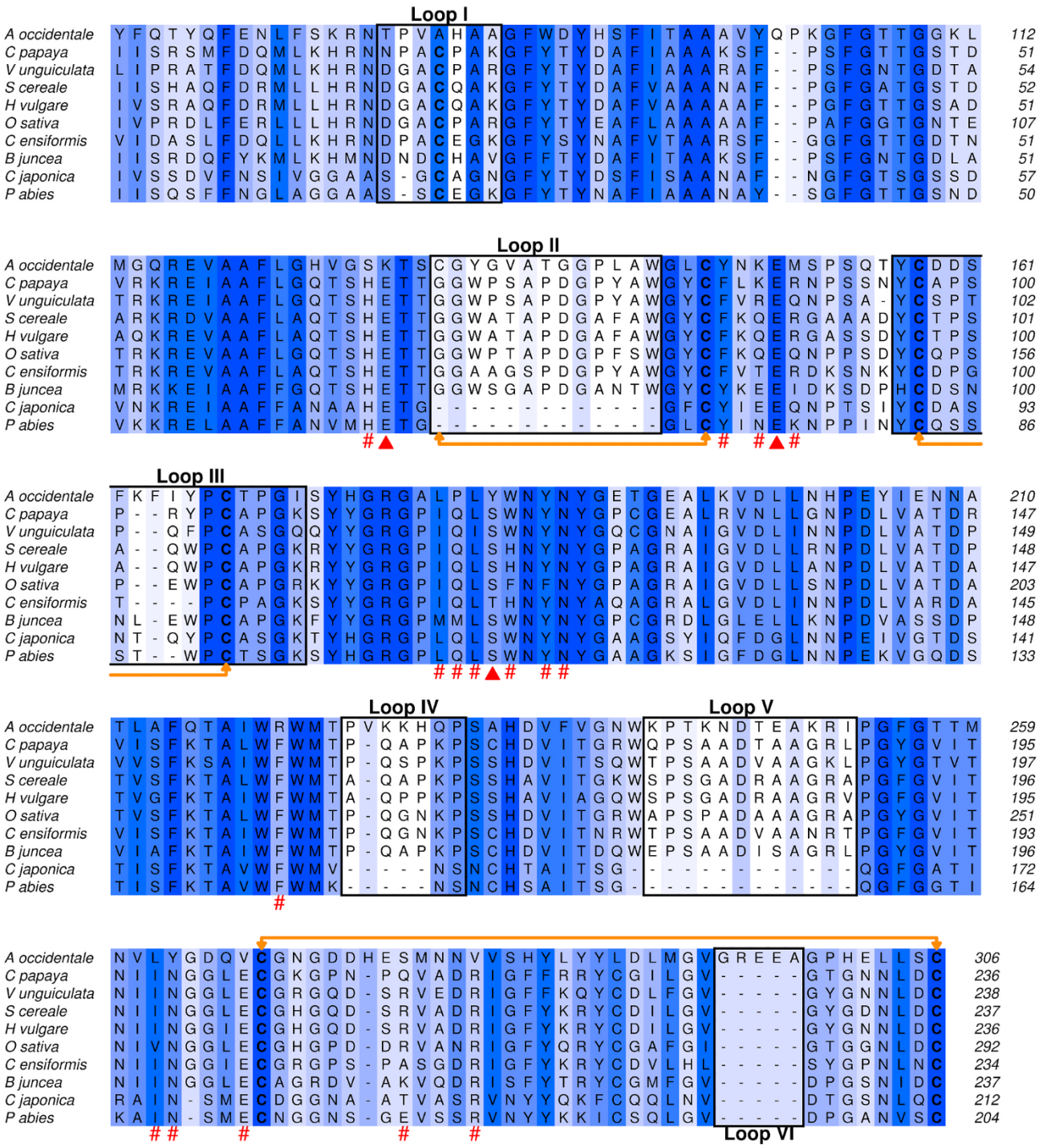

Fig. 3. Alignment of the amino acid sequence of the CatD of AoChi with known three-dimensional structures of GH19 chitinases from plants. The CatD sequence of AoChi was aligned to GH19 structures from: *Carica papaya* (PDB ID: 3CQL), *Vigna unguiculata* subsp. *sesquipedalis* (PDB ID: 4TX7), *Secale cereale* (PDB ID: 4DWX), *Hordeum vulgare* (PDB ID: 2BAA), *Oryza sativa* subsp. *japonica* (PDB ID: 2DKV), *Canavalia ensiformis* (PDB ID: 1DXJ), *Brassica juncea* (PDB ID: 2Z37), *Cryptomeria japonica* (PDB ID: 5H7T) and *Picea abies* (PDB ID: 3HBD). Sites containing residues involved in catalysis (triangles) and substrate-binding (hash marks) are indicated. Disulfide bonds, as observed in the three-dimensional model of AoChi (Fig. 7), are indicated by orange lines. Loop regions (I–V), as assigned by Taira et al. (Taira et al., 2011), are boxed. Loop VI (this work), which is present only in AoChi and other class VI chitinases, is also boxed. Alignment columns are colored according to the ALSCRIPT Calcons convention, as implemented in ALINE (Bond and Schüttelkopf, 2009), using a predefined color scheme, which reflects the conservation of amino acid properties in each column (dark blue: identical residues; white: dissimilar residues). (For interpretation of the references to color in this figure legend, the reader is referred to the Web version of this article.)

mass spectrometry analysis of tryptic peptides from in gel-digestions (Fig. 4B). Eleven peptides, matching specific segments of the primary structure of the recombinant protein (47% coverage), were identified (Figs. S12-S15). One of these peptides confirmed the occurrence of Lys^{128} in the primary structure of the recombinant protein (Table S13). The theoretical molecular mass of the recombinant polypeptide was calculated as 36,428.3 Da (i.e., ~36 kDa), showing that the recombinant protein had an anomalous electrophoretic migration. Both *N*- and *O*-

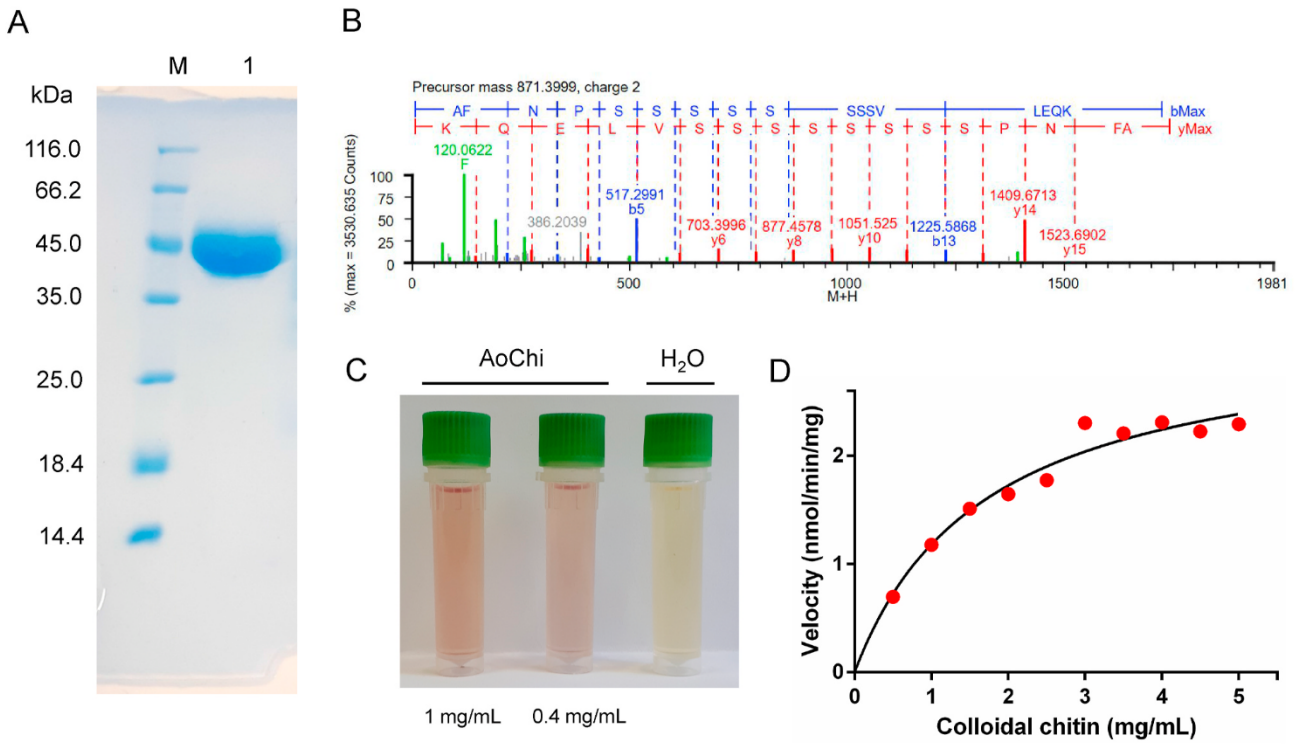

Fig. 4. Polyacrylamide gel electrophoresis (SDS-PAGE) of the purified recombinant chitinase from *Anacardium occidentale*, a member of class VI that has chitinolytic activity. (A) The recombinant chitinase (lane 1; 35 μg) was reduced with β-mercaptoethanol and subjected to denaturing gel electrophoresis (15% polyacrylamide), as described in the Methods section. Lane M: protein markers. (B) Representative fragmentation mass spectrum (LC-MS/MS) of a tryptic peptide, obtained from in gel-digestion of the 45 kDa protein band, that matched a segment of 17 residues of the primary structure of the recombinant product. (C) Colorimetric enzymatic assay, showing the ability of the recombinant cashew chitinase to degrade colloidal chitin. (D) Plot of initial reaction velocities *vs* substrate concentration. The enzymatic assays (panels C and D) were performed at pH 6.0 and 40 °C, and using colloidal chitin as substrate, as described in the Methods section.

glycosylation sites were predicted in the amino acid sequence of cashew chitinase (Fig. S15), which could explain such discrepant values. Supporting this assumption, staining with thymol-sulfuric acid confirmed that AoChi produced in *P. pastoris* is glycosylated (Fig. S16). Indeed, hyper *N*- and *O*-glycosylation of recombinant proteins expressed in *P. pastoris* have been described and characterized, leading in some cases to large differences between theoretical and observed molecular masses of recombinant products (Dionisio et al., 2012; Letourneur et al., 2001).

Far-UV CD spectra of the purified 45 kDa protein produced in *P. pastoris* were characteristic of a folded, α-helical protein (Fig. S17), with two negative bands at 209 nm and 222 nm, separated by a clear and distinct indentation at 215 nm (Holzwarth and Doty, 1965). The purified recombinant cashew protein showed chitinolytic activity, as evidenced by a colorimetric assay using colloidal chitin as substrate (Fig. 4C). Highest hydrolytic activity (>95% relative activity) was observed at temperatures from 30 °C to 50 °C and at pH 6.0 (Fig. 5A and B). The recombinant enzyme was stable over a broad range of pH values, being able to regain its full enzymatic activity when incubated at pH values from 2 to 10 and next incubated at its optimum pH (pH 6.0) for hydrolytic activity (Fig. 5B). Moreover, AoChi retained most of its hydrolytic activity when heated at 60 °C for 1 h. However, the recombinant enzyme exhibited negligible or no detectable chitinolytic activity when incubated for 1 h at temperatures equal or above 70 °C (Fig. 5A and B). Several metal ions (Al^{3+}, Cd^{2+}, Ca^{2+}, Pb^{2+}, Cu^{2+}, Fe^{3+}, Mn^{2+}, Rb^{+} and Zn^{2+}) significantly ($P < 0.05$) reduced AoChi activity, whereas Hg^{2+} completely abolished the enzyme ability to degrade colloidal chitin (Fig. 5C). Metal ions bind to residues at the catalytic sites of chitinases, effectively inhibiting their hydrolytic activity. It has been speculated that the interaction of metal ions with side chain carboxylate groups of critical catalytic residues fix their conformation, restricting their hydrolytic capabilities (Hsieh et al., 2010). Conversely, some cation ions (Ba^{2+}, Cs^{+}, Li^{+}, Ni^{2+} and Ag^{+}) promoted an increase of AoChi activity, but these effects were not significantly different ($P > 0.05$) when compared to the enzymatic activity recorded in the absence of these ions. Increasing concentrations of EDTA, DTT and SDS also caused significant ($P < 0.05$) reductions in AoChi activity (Fig. 5D). When exposed to β-mercaptoethanol, no chitinolytic activity was detected under standard assay conditions (Fig. 5D). These results suggest that AoChi is probably a metalloenzyme, which relies on the presence of cation ions for full activity, and their disulfide bonds play an essential role in maintaining the protein properly folded and hence enzymatically active.

Data of initial reaction rates catalyzed by AoChi *vs* colloidal chitin concentration fitted a hyperbolic curve ($R^2 = 0.9578$), showing the classical Michaelis-Menten kinetics (Fig. 4D). Kinetic parameters were $K_m = 1.71$ mg/mL, $V_{max} = 3.20$ nmol/min/mg, $k_{cat} = 1.15$ min^{-1}, and k_{cat}/K_m (catalytic efficiency) = 0.67 mL mg^{-1} min^{-1}. Values of K_m determined using colloidal chitin for OsChia1b ($K_m = 0.9$ mg/mL), a rice (*Oryza sativa*) class I chitinase, and for OsChia2b ($K_m = 1.9$ mg/mL), a rice class II chitinase (Truong et al., 2003), are in the same order of magnitude when compared to the value determined for AoChi ($K_m = 1.71$ mg/mL). However, V_{max} values of OsChia1b (2.1 μmol/min/mg) and OsChia2b (2.3 μmol/min/mg) are *ca.* 650 to 700-fold higher when compared to the value measured for AoChi ($V_{max} = 3.2$ nmol/min/mg). Kinetic parameters reported for a class IV chitinase from yam (*Dioscorea oppositifolia*), that have been determined using colloidal chitin, were $K_m = 0.518$ mg/mL, $k_{cat} = 0.645$ s^{-1} and $k_{cat}/K_m = 1.25$ mL/mg/s (Arakane et al., 2000). Therefore, although the affinities for the substrate of AoChi and yam chitinase are in the same order of magnitude, turnover number and catalytic efficiency of AoChi (0.020 s^{-1} and 0.012 mL mg s^{-1}) are significantly much lower than those values determined for a class IV chitinase. These distinct kinetic properties of AoChi are likely to be due to the mutations in some residues involved in catalysis, mainly the

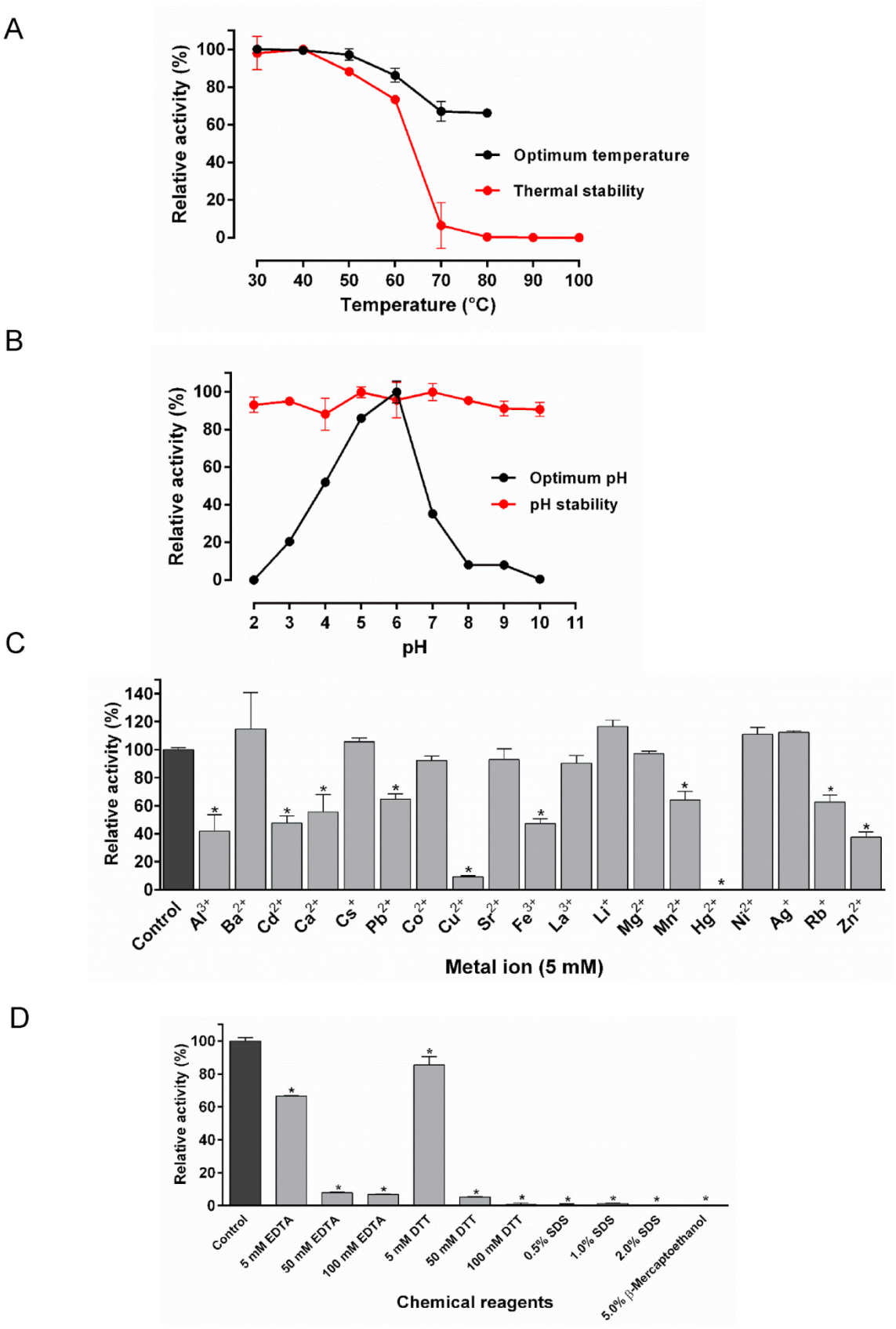

Fig. 5. Effects of temperature (A), pH (B), metal ions (C) and chemical reagents (D) on the hydrolytic activity (A–D) and stability (A–B) of AoChi. Enzymatic assays were performed using the purified recombinant protein (200 μg/mL) and colloidal chitin as substrate, as described in the Methods section. In panels C and D, means that are significantly different ($P < 0.05$; Bonferroni's multiple comparisons test) when compared to control are indicated by asterisks.

replacement of the catalytic Glu for a Lys residue (Lys[128]).

2.3. Antifungal activity of the recombinant cashew chitinase

Lasiodiplodia theobromae is a phytopathogenic, filamentous fungus (Ascomycota) of the family Botryosphaeriaceae, that has a wide range of host plants in tropical and subtropical regions. It can cause different diseases such as dieback, root rot, blights and gummosis (Muniz et al., 2011). To test if AoChi could inhibit the growth of this important phytopathogen, *in vitro* assays were performed using an isolate of

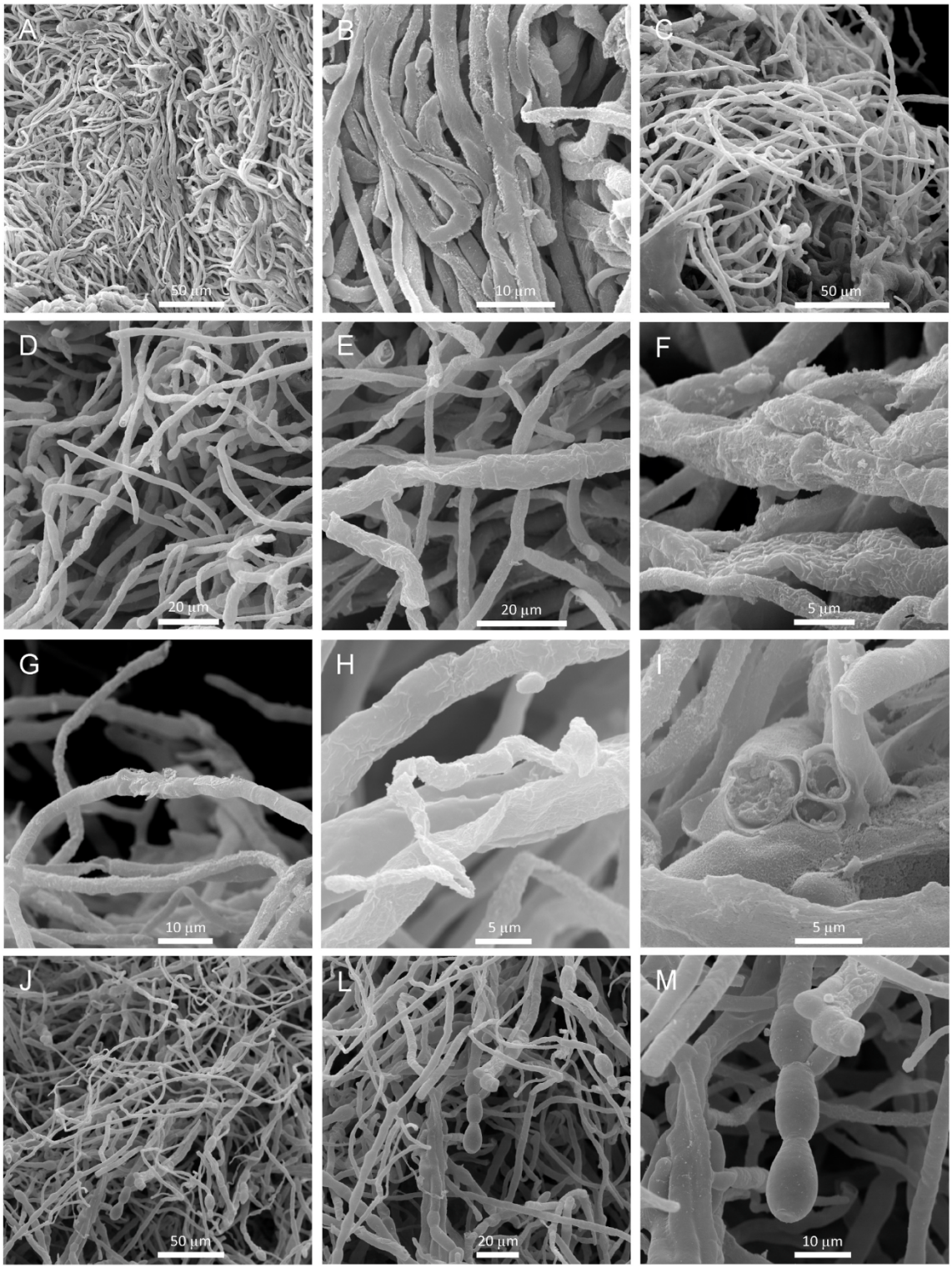

Fig. 6. Morphological alterations induced in *Lasiodiplodia theobromae* hyphae by *Anacardium occidentale* chitinase. SEM images of untreated mycelium(A-B), mycelium treated with 500 µg AoChi (C–I) and mycelium treated with 5 µg Carbendazim (J–M) are shown. The assays to evaluate the morphological alterations in *L. theobromae* grown *in vitro* in the presence of AoChi and acquisition of SEM images were performed as described in the Methods section. SEM images from fungus grown in the presence of water (A–B) or Carbendazim (J–M) were included for comparison.

L. theobromae infecting banana fruits (Fig. S18). When the fungus was exposed to a dose of 500 μg of AoChi, a delay in mycelium growth was clearly observed (Fig. S19). The inhibitory effect of AoChi on the mycelial growth of *L. theobromae* was observed until 72 h after the beginning of the assay (Fig. S20), representing an inhibition index of 53.3%. SEM images of fungus mycelium treated with AoChi revealed that the recombinant protein induced several and notable morphological alterations (Fig. 6). Hyphae of untreated mycelium had a normal appearance, characterized by a dense network of long, interwoven, tubular structures, displaying a smooth, uniform surface (Fig. 6A and B). On the other hand, mycelia that were exposed to AoChi exhibited a disorganized array of shorter and thinner hyphae, showing several morphological alterations (Fig. 6C–I) Most frequent morphological alterations induced by AoChi included: *i*) hyphae with moniliform appearance, characterized by adjacent swollen segments; *ii*) flat, ribbon-shaped hyphae, some of them appearing as empty, squashed, translucent tubes; *iii*) and wrinkled, collapsed hyphae exhibiting a rough surface. In some images, it could be observed that the outer layer of the cell wall from hyphae of *L. theobromae* exposed to AoChi was peeling off (Fig. 6H). Moreover, alterations in hyphal tips were also observed, which usually appeared swollen, forming sometimes large bulges (Fig. 6C and D). Some hyphae were found broken, appearing like a round end tube whose border was perpendicularly chopped with a sharp blade, producing a regular, flat edge (Fig. 6I). These results showed that AoChi was able to inhibit the growth of a phytopathogenic fungus, inducing several morphological alterations in hyphae and hyphal tips, as revealed by SEM analysis. Therefore, although AoChi possesses distinct structural features in comparison to classical GH19 plant chitinases, it exhibits the ability to inhibit *in vitro* fungal growth, causing hyphae morphological alterations, similarly to what has been found for the antifungal chitinases RSC-a (rye seed chitinase-a) from class I, RSC-c (rye seed chitinase-c) from class II and yam chitinase from class IV (Karasuda et al., 2003; Taira et al., 2002). The morphological alterations induced by AoChi in both hyphal tips and lateral mature walls of *L. lasiodiplodia* agree with previous findings reported by Taira et al. (2002), who showed that when *Trichoderma* sp. was incubated with FITC-labeled RSC-a, the fluorescent protein was found located in hyphal tips, lateral walls and septa. Probably, the antifungal action of AoChi is due to hydrolysis of nascent chitin chains in the tips of growing hyphal branches as well as to degradation of mature chitin fibers in lateral cell walls.

2.4. A molecular mechanism for the chitinolytic and antifungal properties of A. occidentale class VI chitinase

To investigate a probable mechanism for the chitinolytic and antifungal properties of cashew class VI chitinase, a three-dimensional molecular model of its GH19 domain was generated by homology modeling (Fig. S21), the model was validated (Fig. S22 and Table S3) and molecular docking calculations were performed, in which a $(GlcNAc)_4$ oligosaccharide was docked in the substrate-binding cleft of AoChi (Fig. 7). The three-dimensional model of AoChi showed the typical features of GH19 structures, with 11 α-helixes, several loop regions connecting the helical segments and 3 disulfide bonds (Fig. 7A). The replacement of a conserved Cys residue by Ala (Ala^{82}) was compensated by the emergence of a new Cys residue (Cys^{131}), and this new Cys residue was predicted to establish a disulfide bond with Cys^{146}, thus maintaining the conserved number of 3 disulfide linkages, a typical structural feature of plant GH19 chitinases (Fig. 7A).

Once the overall characteristics of the AoChi three-dimensional model were analyzed as well as the quality of its local and global stereo-chemical parameters were assessed, a chito-oligosaccharide with 4 units of GlcNAc was docked in the substrate-binding cleft of the validated model. The complex protein-carbohydrate was predicted to be stabilized by a network of hydrogen bonds, involving O and N atoms of the side chains of certain AoChi residues and O atoms of hydroxyl and carbonyl groups of the sugar units as well as the O atoms of the glycosidic bonds, linking the GlcNAc units of the oligosaccharide (Fig. 7B). The side chain of Lys^{128}, which replaces the conserved Glu that acts as the proton donor in classical chitinases, was directed towards the ligand. The side chain of Glu^{150}, the putative general base, was on the opposite side of the substrate-binding cleft. The distances between the Nζ atom of Lys^{128} and the atoms Oε1 and Oε2 of Glu^{150} were 8.0 Å and 7.9 Å. The relative positions of the side chains of Lys^{128} and Glu^{150} as well as the average distance between their Nζ and Oε atoms agree to what is usually observed for the positions and average distances between the catalytic carboxyl groups in several structures of inverting GHs (Mhlongo et al., 2014). Furthermore, the distance between the Nζ atom of Lys^{128} and the most probable scissile *O*-glycosidic bond in the oligosaccharide docked in the substrate-binding groove of AoChi (approximately 4 Å), suggests that Lys^{128} could act as the proton donor during catalysis. Supporting this assumption, the theoretical pK_a value of the ζNH_3^+ group of Lys^{128}, as predicted using the software PROPKA3, was 6.01, whereas the pK_a for the δCOOH group of the general base Glu^{150} was calculated as 4.48 (Table S4). These numbers corroborate the enzymatic activity profile of AoChi as a function of pH values (Fig. 5B). A rapid, exponential-like increase in AoChi activity was observed from pH 3.0 to pH 5.0. This could be due to the continuous increase in the deprotonated form of the carboxyl group of Glu^{150}, acting as a base, and the concomitant deprotonation of the ζNH_3^+ group of Lys^{128}, acting as the proton donor. On the other hand, AoChi activity rapidly decreased beyond pH 6.0, reaching negligible values at pH 8.0. At pH 8.0, most (~99%) ζNH_3^+ groups of Lys^{128} residues would be in a deprotonated form, and thus could no longer act as proton donors to sustain catalysis.

The CatD of AoChi has, besides Lys^{128}, another 11 Lys residues, all of them with theoretical pK_a values of their ζNH_3^+ groups ranging from 10.18 (Lys^{76}) to 10.75 (Lys^{111}). The average experimental pK_a values for Lys residues, measured in 157 proteins, have been determined to be 10.68 (Pahari et al., 2019), which is close to the intrinsic pK_a of the ζNH_3^+ group of Lys in bulk water, which is 10.4 (Nozaki and Tanford, 1967). However, Lys and other ionizable residues buried in the hydrophobic environments of certain proteins might have anomalous pK_a values, with large deviations from the intrinsic pK_a values in water. Indeed, buried Lys residues with experimental pK_a values as low as 6.2 have been experimentally determined (Kougentakis et al., 2018). Therefore, this analysis supports the assumption that Lys^{128} of AoChi can act as the proton donor during catalysis, explaining the ability of *A. occidentale* class VI chitinase to degrade colloidal chitin and to cause damages in the cell walls of pathogenic fungi.

3. Conclusions

Despite the replacement of a critical catalytic Glu for a Lys residue, a class VI chitinase from *Anacardium occidentale* has preserved the ability to degrade chitin, although showing lower turnover number and catalytic efficiency in comparison to typical GH19 enzymes. Cashew class VI chitinase has also showed the capacity to inhibit the growth of a pathogenic fungus (*Lasiodiplodia theobromae*), inducing extensive alterations in hyphae morphology. The results of the present work suggest that class VI chitinases have accumulated adaptive mutations that are likely important for the role these proteins have in fundamental biological processes related to plant growth and development. Even so, they have preserved their chitinolytic and antifungal properties, and probably act as bifunctional enzymes in plant biology.

4. Experimental

4.1. Plant material

Nuts from CCP 76, a dwarf clone of *Anacardium occidentale* L. (Fig. S1A), were provided by Embrapa (Brazilian Agricultural Research Corporation) Tropical Agroindustry, Fortaleza, Ceará, Brazil. Seeds were sown in sandy soil, in 400 mL plastic pots, which were kept under

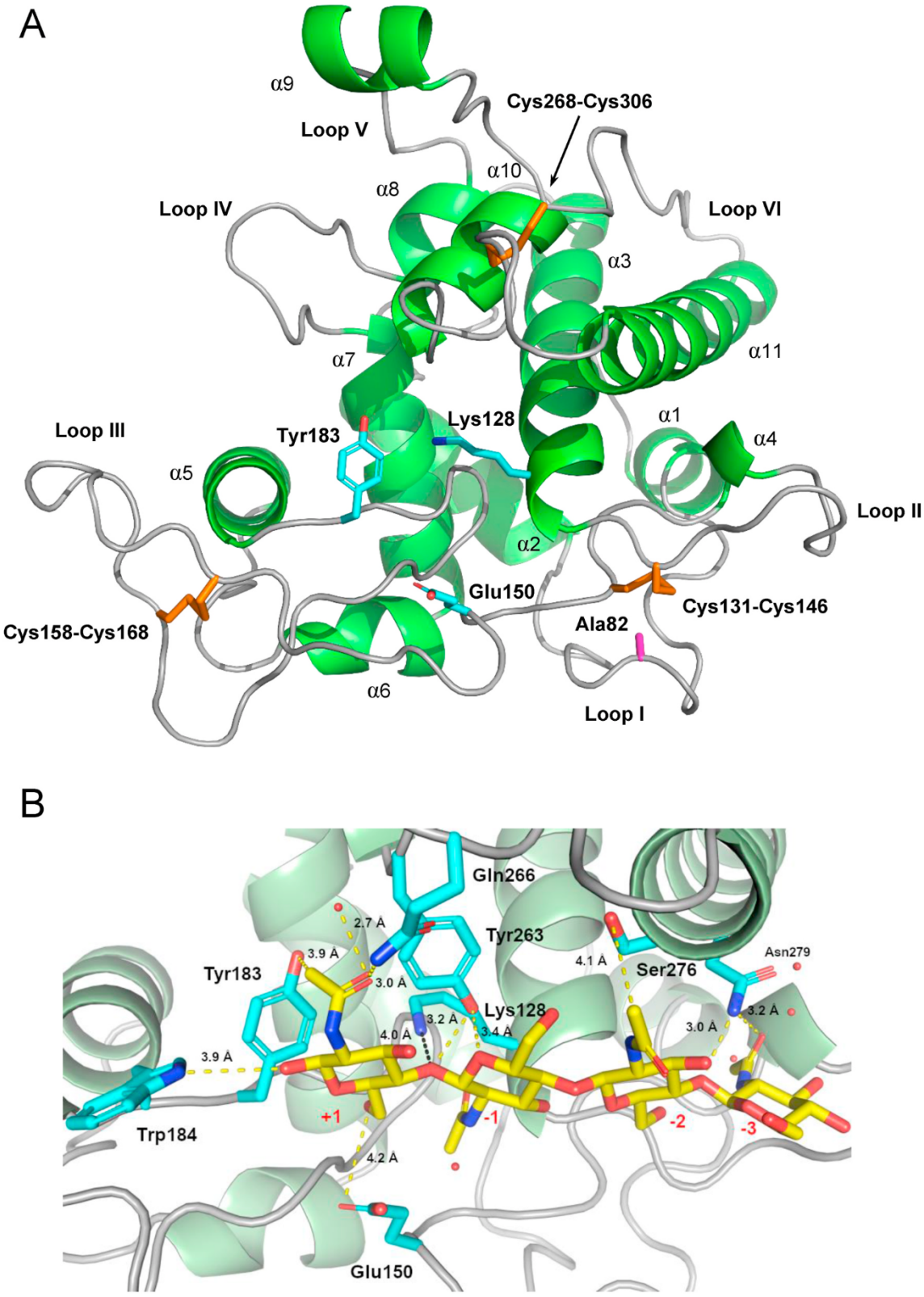

Fig. 7. Three-dimensional molecular model of AoChi and its interaction with a chitin oligomer. (A) Cartoon representation of the three-dimensional molecular model of AoChi, which was generated by homology modeling. Side chains of putative catalytic residues are shown as sticks. Disulfide bonds are colored orange. (B) Detailed view of a chito-oligosaccharide (yellow) docked in the substrate-binding cleft of AoChi. Side chains of AoChi residues that probably interact with the docked ligand through hydrogen bonds (represented as yellow dotted lines) are shown as sticks (cyan). N and O atoms are colored blue and red, respectively. (For interpretation of the references to color in this figure legend, the reader is referred to the Web version of this article.)

greenhouse conditions and irrigated daily with tap water. Leaves of 60-day old plants (Fig. S1B) were harvested, immediately frozen in liquid nitrogen and used for nucleic acids purification.

4.2. Cells, plasmids, culture media and chemical reagents

Bacterial (*Escherichia coli* DH5α) and yeast (*P. pastoris* KM71H) cells as well as the plasmid pPICZαA were purchased from Invitrogen (Carlsbad, CA, USA). The plasmid pGEM-T Easy was purchased from Promega (Madison, WI, USA). Bacterial cells were cultivated in LB broth and low salt LB, whereas yeast cells were cultivated in YPD, YPDS, BMGY and BMMY. Culture media were prepared as previously described (Landim et al., 2017). All other reagents were of analytical, high purity grade.

4.3. Purification of nucleic acids

Genomic DNA and total RNA were purified using the CTAB-based protocols described by Warner (1996) and Chang et al. (1993), respectively. Integrity of nucleic acid samples was evaluated by agarose gel electrophoresis, and their concentrations were determined by measuring the absorbance at 260 nm, as previously described (Sambrook et al., 1989).

4.4. cDNA synthesis, amplification, cloning and sequencing

Total RNA (1 μg) was treated with RNase-free DNase I and subjected to first-strand cDNA synthesis using an oligo$(dT)_{20}$ primer and the ImProm-II reverse transcriptase (Promega), according to the protocol supplied by the enzyme's manufacturer. Next, a cDNA fragment encoding the mature form of a GH19 cashew chitinase was amplified by PCR using specific oligonucleotide primers, which were designed based on a cDNA sequence obtained from cashew mRNA (GenBank accession number: MN623695; Fig. S2). The primer sequences were: 5′-GAATTCGATGGAGAAATGCCATCC-3′ (forward) and 5′-TCTAGAACA-GAAGATGACGAGGAAGAAG-3′ (reverse). Sites for the restriction endonucleases *Eco*RI and *Xba*I were included in the 5′ ends of the forward and reverser primers, respectively, to allow the manipulation of the amplicon. Amplification reactions (25 μL final volume) contained: DNA template, 200 μM each dNTP, 0.2 μM each primer, 1.5 mM $MgCl_2$, 1 × reaction buffer, and 1 U *Taq* DNA polymerase (GE Healthcare Life Sciences, Uppsala, Sweden). The following cycling parameters were used: an initial denaturation step (95 °C for 4 min) followed by 35 cycles of denaturation (95 °C for 45 s), annealing (63 °C for 1 min) and extension (72 °C for 2 min). After the last cycle, reactions were incubated at 72 °C for 8 min, cooled to 4 °C and subjected to agarose gel electrophoresis (Fig. S3). Cloning of amplified cDNA fragments into the pGEM-T Easy vector, selection of *E. coli* DH5α cells harboring the recombinant plasmid and DNA sequencing and assembly of the inserts from random selected clones were performed essentially as described by Landim et al. (2017).

4.5. Construction of the expression vector and selection of transformed P. pastoris cells

A cDNA fragment encoding cashew chitinase (Figs. S8 and S9) was subcloned from pGEM-T Easy into the pPICZαA vector using the sites for *Eco*RI and *Xba*I, and the recombinant plasmid was propagated in *E. coli* DH5α, linearized with *Sac*I and introduced in *P. pastoris* KM71H cells by electroporation, according to the protocols described in the EasySelect™ *Pichia* Expression Kit user manual (http://tools.invitrogen.com/content/sfs/manuals/easyselect_man.pdf). The identification of *P. pastoris* transformants containing the expression cassette (P_{AOX1}-pre-proαMF-*Ao*Chi-6 × His-*myc* epitope-TT_{AOX1}-*Sh ble*) integrated at the *AOX1* locus was performed as previously described (Landim et al., 2017).

4.6. Expression and purification of the recombinant cashew chitinase

Transformed cells of *P. pastoris* KM71H were cultivated in BMMY containing 100 μg/mL zeocin and 0.5% (v/v) methanol for 144 h, as described by Landim et al. (2017). Induced cultures were centrifuged (3000 *g* at 4 °C for 5 min) and the cell-free supernatant was dialyzed against distilled water and subjected to fractionation with solid ammonium sulfate. Proteins fractionated between 35 and 95% saturation (F35/95) were dialyzed against distilled water and the recombinant protein was purified by immobilized metal affinity chromatography (IMAC), as previously described (Sousa et al., 2019).

4.7. Protein analysis

Soluble protein content was determined using the Bradford method (Bradford, 1976). The electrophoretic profile of protein samples was determined by polyacrylamide gel electrophoresis under denaturing conditions (SDS-PAGE), as described by Laemmli (1970), using 15% polyacrylamide slab gels (Lobo et al., 2013). Protein bands were visualized using colloidal Coomassie Brilliant Blue G-250 staining (Dyballa and Metzger, 2009). Detection of glycoproteins resolved by SDS-PAGE was performed using the thymol-sulfuric acid method, as described by Racusen (1979). Identification of tryptic peptides from protein bands resolved by SDS-PAGE was performed using tandem mass spectrometry (LC-ESI-MS/MS), as described in detail by Rocha et al. (2018).

4.8. Colorimetric enzymatic assay

Chitinase activity was determined using colloidal chitin as substrate, which was prepared using the method described by Molano et al. (1977). The enzymatic assay was performed as previously described (Lobo et al., 2013). One unit (U) of chitinolytic activity was defined as the amount of enzyme that released 1 nmol of GlcNAc/mL/h, under specified assay conditions.

4.9. Biochemical characterization of the recombinant chitinase

Optimal values of temperature and pH for chitinase activity, stability to different values of temperature and pH, and the effects of metal ions and chemical reagents on enzymatic activity were determined as described by Lobo et al. (2013). Steady-state kinetic parameters of AoChi were determined using colloidal chitin as substrate, at concentrations varying from 0.5 to 5 mg/mL. The assays were performed at pH 6.0 (protein dissolved 50 mM sodium acetate buffer) and 40 °C. Michaelis-Menten constant (K_m), maximal reaction velocity (V_{max}) and the turnover number (k_{cat}) were calculated from plots of initial rates *vs* substrate concentration, using GraphPad Prism software v.6.01. Far-UV circular dichroism (CD) spectra of AoChi were acquired using a Jasco J-815 spectropolarimeter (Jasco International Co., Tokyo, Japan), as described by Carneiro et al. (2017).

4.10. Evaluation of the antifungal activity of cashew chitinase

The effect of the purified chitinase (3.7 mg/mL, dissolved in water) on the growth of an isolate of *Lasiodiplodia theobromae* infecting banana fruits (Fig. S18) was evaluated *in vitro*. Protein samples (dose = 500 μg) were spread on the surface of PDA (potato dextrose agar medium) plates (3 replicates per dose) using a Drigalski spatula and incubated at room temperature for 10 min. Next, a small disc (~10 mm diameter) containing fungus mycelium was placed on the center of each plate and the plates were incubated at 28 °C ± 2 °C and photoperiod of 12 h light/12 h darkness. Mycelial growth was monitored and photographed at every 24 h. Mycelium discs inoculated on plates in which water or Carbendazim (Derosal 500 SC, Bayer) were spread over the medium were used as controls. To investigate possible morphological alterations of fungal hyphae exposed to AoChi, samples of treated mycelia were subjected to

scanning electron microscopy (SEM). Samples preparation and images acquisition were performed as described elsewhere (Holanda et al., 2019).

4.11. Homology modeling and molecular docking

Homology modeling was performed using the Phyre2 web portal (Kelley et al., 2015). The stereo-chemical quality of the molecular model of AoChi was evaluated using PROSESS (Berjanskii et al., 2010). Molecular docking calculations were performed using AutoDock Tools v. 1.5.6 (Morris et al., 2009) and AutoDock Vina v. 1.1.2 (Trott and Olson, 2010), as previously described (Maranhão et al., 2017).

Declaration of competing interest

The authors declare that they have no known competing financial interests or personal relationships that could have appeared to influence the work reported in this paper.

Acknowledgements

This work was supported by research grants from Conselho Nacional de Desenvolvimento Científico e Tecnológico (CNPq) and Coordenação de Aperfeiçoamento de Pessoal de Nível Superior (CAPES). STO was recipient of a Doctoral Fellowship from CAPES.

Appendix A. Supplementary data

Supplementary data to this article can be found online at https://doi.org/10.1016/j.phytochem.2020.112527.

References

Arakane, Y., Hoshika, H., Kawashima, N., Fujiya-Tsujimoto, C., Sasaki, Y., Koga, D., 2000. Comparison of chitinase isozymes from yam tuber–enzymatic factor controlling the lytic activity of chitinases. Biosci. Biotechnol. Biochem. 64, 723–730. https://doi.org/10.1271/bbb.64.723.

Berjanskii, M., Liang, Y., Zhou, J., Tang, P., Stothard, P., Zhou, Y., Cruz, J., MacDonell, C., Lin, G., Lu, P., Wishart, D.S., 2010. PROSESS: a protein structure evaluation suite and server. Nucleic Acids Res. 38, W633–W640. https://doi.org/10.1093/nar/gkq375.

Bond, C.S., Schüttelkopf, A.W., 2009. ALINE: a WYSIWYG protein-sequence alignment editor for publication-quality alignments. Acta Crystallogr. D Biol. Crystallogr. 65, 510–512. https://doi.org/10.1107/S0907444909007835.

Bradford, M.M., 1976. A rapid and sensitive method for the quantitation of microgram quantities of protein utilizing the principle of protein-dye binding. Anal. Biochem. 72, 248–254.

Brameld, K.A., Goddard, W.A., 1998. The role of enzyme distortion in the single displacement mechanism of family 19 chitinases. Proc. Natl. Acad. Sci. U.S.A. 95, 4276–4281.

Carneiro, R.F., Torres, R.C.F., Chaves, R.P., de Vasconcelos, M.A., de Sousa, B.L., Goveia, A.C.R., Arruda, F.V., Matos, M.N.C., Matthews-Cascon, H., Freire, V.N., Teixeira, E.H., Nagano, C.S., Sampaio, A.H., 2017. Purification, biochemical characterization, and amino acid sequence of a novel type of lectin from *Aplysia dactylomela* eggs with antibacterial/antibiofilm potential. Mar. Biotechnol. 19, 49–64. https://doi.org/10.1007/s10126-017-9728-x.

Chang, S., Puryear, J., Cairney, J., 1993. A simple and efficient method for isolating RNA from pine trees. Plant Mol. Biol. Rep. 11, 113–116. https://doi.org/10.1007/BF02670468.

Collinge, D.B., Kragh, K.M., Mikkelsen, J.D., Nielsen, K.K., Rasmussen, U., Vad, K., 1993. Plant chitinases. Plant J. 3, 31–40. https://doi.org/10.1046/j.1365-313x.1993.t01-1-00999.x.

Crini, G., 2019. Historical review on chitin and chitosan biopolymers. Environ. Chem. Lett. 17, 1623–1643. https://doi.org/10.1007/s10311-019-00901-0.

Dionisio, G., Jørgensen, M., Welinder, K.G., Brinch-Pedersen, H., 2012. Glycosylations and truncations of functional cereal phytases expressed and secreted by *Pichia pastoris* documented by mass spectrometry. Protein Expr. Purif. 82, 179–185. https://doi.org/10.1016/j.pep.2011.12.003.

Dyballa, N., Metzger, S., 2009. Fast and sensitive colloidal coomassie G-250 staining for proteins in polyacrylamide gels. JoVE e1431. https://doi.org/10.3791/1431.

Fukamizo, T., Koga, D., Goto, S., 1995. Comparative biochemistry of chitinases—anomeric form of the reaction products. Biosci. Biotechnol. Biochem. 59, 311–313. https://doi.org/10.1271/bbb.59.311.

Gonzalez, L.M.G., El Kayal, W., Morris, J.S., Cooke, J.E.K., 2015. Diverse chitinases are invoked during the activity-dormancy transition in spruce. Tree Genet. Genomes 11, 41. https://doi.org/10.1007/s11295-015-0871-0.

Gow, N.A.R., Latge, J.-P., Munro, C.A., 2017. The fungal cell wall: structure, biosynthesis, and function. Microbiol. Spectr. 5 https://doi.org/10.1128/microbiolspec.FUNK-0035-2016.

Hart, P.J., Pfluger, H.D., Monzingo, A.F., Hollis, T., Robertus, J.D., 1995. The refined crystal structure of an endochitinase from *Hordeum vulgare* L. seeds at 1.8 A resolution. J. Mol. Biol. 248, 402–413.

Holanda, A.E.R., Souza, B.C., Carvalho, E.C.D., Oliveira, R.S., Martins, F.R., Muniz, C.R., Costa, R.C., Soares, A.A., 2019. How do leaf wetting events affect gas exchange and leaf lifespan of plants from seasonally dry tropical vegetation? Plant Biol. 21, 1097–1109. https://doi.org/10.1111/plb.13023.

Holzwarth, G., Doty, P., 1965. The ultraviolet circular dichroism of polypeptides. J. Am. Chem. Soc. 87, 218–228. https://doi.org/10.1021/ja01080a015.

Hossain, M.A., Noh, H.-N., Kim, K.-I., Koh, E.-J., Wi, S.-G., Bae, H.-J., Lee, H., Hong, S.-W., 2010. Mutation of the chitinase-like protein-encoding AtCTL2 gene enhances lignin accumulation in dark-grown *Arabidopsis* seedlings. J. Plant Physiol. 167, 650–658. https://doi.org/10.1016/j.jplph.2009.12.001.

Hsieh, Y.-C., Wu, Y.-J., Chiang, T.-Y., Kuo, C.-Y., Shrestha, K.L., Chao, C.-F., Huang, Y.-C., Chuankhayan, P., Wu, W.-G., Li, Y.-K., Chen, C.-J., 2010. Crystal structures of *Bacillus cereus* NCTU2 chitinase complexes with chitooligomers reveal novel substrate binding for catalysis: a chitinase without chitin binding and insertion domains. J. Biol. Chem. 285, 31603–31615.

Iseli, B., Armand, S., Boller, T., Neuhaus, J.M., Henrissat, B., 1996. Plant chitinases use two different hydrolytic mechanisms. FEBS Lett. 382, 186–188. https://doi.org/10.1016/0014-5793(96)00174-3.

Johnson, D., 1973. The botany, origin, and spread of the cashew *Anacardium occidentale* L. J. Plant. Crops 1, 1–7.

Karasuda, S., Tanaka, S., Kajihara, H., Yamamoto, Y., Koga, D., 2003. Plant chitinase as a possible biocontrol agent for use instead of chemical fungicides. Biosci. Biotechnol. Biochem. 67, 221–224. https://doi.org/10.1271/bbb.67.221.

Kelley, L.A., Mezulis, S., Yates, C.M., Wass, M.N., Sternberg, M.J.E., 2015. The Phyre2 web portal for protein modeling, prediction and analysis. Nat. Protoc. 10, 845–858. https://doi.org/10.1038/nprot.2015.053.

Kesari, P., Patil, D.N., Kumar, Pramod, Tomar, S., Sharma, A.K., Kumar, Pravindra, 2015. Structural and functional evolution of chitinase-like proteins from plants. Proteomics 15, 1693–1705. https://doi.org/10.1002/pmic.201400421.

Kolosova, N., Breuil, C., Bohlmann, J., 2014. Cloning and characterization of chitinases from interior spruce and lodgepole pine. Phytochemistry 101, 32–39. https://doi.org/10.1016/j.phytochem.2014.02.006.

Kougentakis, C.M., Grasso, E.M., Robinson, A.C., Caro, J.A., Schlessman, J.L., Majumdar, A., García-Moreno, E.B., 2018. Anomalous properties of Lys residues buried in the hydrophobic interior of a protein revealed with 15N-detect NMR spectroscopy. J. Phys. Chem. Lett. 9, 383–387. https://doi.org/10.1021/acs.jpclett.7b02668.

Kumar, S., Stecher, G., Li, M., Knyaz, C., Tamura, K., 2018. Mega X: molecular evolutionary genetics analysis across computing platforms. Mol. Biol. Evol. 35, 1547–1549. https://doi.org/10.1093/molbev/msy096.

Laemmli, U.K., 1970. Cleavage of structural proteins during the assembly of the head of bacteriophage T4. Nature 227, 680–685.

Landim, P.G.C., Correia, T.O., Silva, F.D.A., Nepomuceno, D.R., Costa, H.P.S., Pereira, H. M., Lobo, M.D.P., Moreno, F.B.M.B., Brandão-Neto, J., Medeiros, S.C., Vasconcelos, I.M., Oliveira, J.T.A., Sousa, B.L., Barroso-Neto, I.L., Freire, V.N., Carvalho, C.P.S., Monteiro-Moreira, A.C.O., Grangeiro, T.B., 2017. Production in *Pichia pastoris*, antifungal activity and crystal structure of a class I chitinase from cowpea (*Vigna unguiculata*): insights into sugar binding mode and hydrolytic action. Biochimie 135, 89–103. https://doi.org/10.1016/j.biochi.2017.01.014.

Letourneur, O., Gervasi, G., Gaïa, S., Pagès, J., Watelet, B., Jolivet, M., 2001. Characterization of *Toxoplasma gondii* surface antigen 1 (SAG1) secreted from Pichia pastoris: evidence of hyper O-glycosylation. Biotechnol. Appl. Biochem. 33, 35–45. https://doi.org/10.1042/ba20000069.

Liu, X., Zhang, J., Zhu, K.Y., 2019. Chitin in arthropods: biosynthesis, modification, and metabolism. Adv. Exp. Med. Biol. 1142, 169–207. https://doi.org/10.1007/978-981-13-7318-3_9.

Lobo, M.D., Silva, F.D., Landim, P.G., da Cruz, P.R., de Brito, T.L., de Medeiros, S.C., Oliveira, J.T., Vasconcelos, I.M., Pereira, H.D., Grangeiro, T.B., 2013. Expression and efficient secretion of a functional chitinase from *Chromobacterium violaceum* in *Escherichia coli*. BMC Biotechnol. 13, 46. https://doi.org/10.1186/1472-6750-13-46.

Lombard, V., Golaconda Ramulu, H., Drula, E., Coutinho, P.M., Henrissat, B., 2014. The carbohydrate-active enzymes database (CAZy) in 2013. Nucleic Acids Res. 42, D490–D495. https://doi.org/10.1093/nar/gkt1178.

Maranhão, P.A.C., Teixeira, C.S., Sousa, B.L., Barroso-Neto, I.L., Monteiro-Júnior, J.E., Fernandes, A.V., Ramos, M.V., Vasconcelos, I.M., Gonçalves, J.F.C., Rocha, B.A.M., Freire, V.N., Grangeiro, T.B., 2017. cDNA cloning, molecular modeling and docking calculations of L-type lectins from *Swartzia simplex* var. *grandiflora* (Leguminosae, Papilionoideae), a member of the tribe Swartzieae. Phytochemistry 139, 60–71. https://doi.org/10.1016/j.phytochem.2017.04.007.

Margis-Pinheiro, M., Metz-Boutigue, M.H., Awade, A., de Tapia, M., le Ret, M., Burkard, G., 1991. Isolation of a complementary DNA encoding the bean PR4 chitinase: an acidic enzyme with an amino-terminus cysteine-rich domain. Plant Mol. Biol. 17, 243–253. https://doi.org/10.1007/bf00039499.

Mayes, H.B., Knott, B.C., Crowley, M.F., Broadbelt, L.J., Ståhlberg, J., Beckham, G.T., 2016. Who's on base? Revealing the catalytic mechanism of inverting family 6 glycoside hydrolases. Chem. Sci. 7, 5955–5968. https://doi.org/10.1039/c6sc00571c.

Mhlongo, N.N., Skelton, A.A., Kruger, G., Soliman, M.E.S., Williams, I.H., 2014. A critical survey of average distances between catalytic carboxyl groups in glycoside hydrolases. Proteins 82, 1747–1755. https://doi.org/10.1002/prot.24528.

Mir, Z.A., Ali, S., Shivaraj, S.M., Bhat, J.A., Singh, A., Yadav, P., Rawat, S., Paplao, P.K., Grover, A., 2020. Genome-wide identification and characterization of Chitinase gene family in *Brassica juncea* and *Camelina sativa* in response to *Alternaria brassicae*. Genomics 112, 749–763. https://doi.org/10.1016/j.ygeno.2019.05.011.

Molano, J., Durán, A., Cabib, E., 1977. A rapid and sensitive assay for chitinase using tritiated chitin. Anal. Biochem. 83, 648–656.

Morris, G.M., Huey, R., Lindstrom, W., Sanner, M.F., Belew, R.K., Goodsell, D.S., Olson, A.J., 2009. AutoDock4 and AutoDockTools4: automated docking with selective receptor flexibility. J. Comput. Chem. 30, 2785–2791. https://doi.org/10.1002/jcc.21256.

Muniz, C.R., Freire, F.C.O., Viana, F.M.P., Cardoso, J.E., Cooke, P., Wood, D., Guedes, M. I.F., 2011. Colonization of cashew plants by *Lasiodiplodia theobromae*: microscopical features. Micron 42, 419–428. https://doi.org/10.1016/j.micron.2010.12.003.

Neuhaus, J.M., 1999. Plant chitinases (PR-3, PR-4, PR-8, PR-11). In: Datta, S.K., Muthukrishnan, S. (Eds.), Pathogenesis Related Proteins in Plants. CRC Press LLC, Boca Raton, pp. 77–105.

Nozaki, Y., Tanford, C., 1967. Acid-base titrations in concentrated guanidine hydrochloride. Dissociation constants of the guamidinium ion and of some amino acids. J. Am. Chem. Soc. 89, 736–742. https://doi.org/10.1021/ja00980a002.

Pahari, S., Sun, L., Alexov, E., 2019. PKAD: a database of experimentally measured pKa values of ionizable groups in proteins. Database 2019, baz024. https://doi.org/10.1093/database/baz024.

Racusen, D., 1979. Glycoprotein detection in polyacrylamide gel with thymol and sulfuric acid. Anal. Biochem. 99, 474–476. https://doi.org/10.1016/s0003-2697(79)80035-4.

Rita Marques, M., Xavier-Filho, J., 1991. Enzymatic and inhibitory activities of cashew tree gum exudate. Phytochemistry 30, 1431–1433. https://doi.org/10.1016/0031-9422(91)84179-V.

Rocha, A.J., Sousa, B.L., Girão, M.S., Barroso-Neto, I.L., Monteiro-Júnior, J.E., Oliveira, J.T.A., Nagano, C.S., Carneiro, R.F., Monteiro-Moreira, A.C.O., Rocha, B.A. M., Freire, V.N., Grangeiro, T.B., 2018. Cloning of cDNA sequences encoding cowpea (*Vigna unguiculata*) vicilins: computational simulations suggest a binding mode of cowpea vicilins to chitin oligomers. Int. J. Biol. Macromol. 117, 565–573. https://doi.org/10.1016/j.ijbiomac.2018.05.197.

Sambrook, J., Fritsch, E., Maniatis, T., 1989. Molecular Cloning: A Laboratory Manual, second ed. Cold Spring Harbor Laboratory Press, Cold Spring Harbor.

Shinshi, H., Neuhas, J.M., Ryals, J., Meins, F., 1990. Structure of a tobacco endochitinase gene: evidence that different chitinase genes can arise by transposition of sequences encoding a cysteine-rich domain. Plant Mol. Biol. 14, 357–368. https://doi.org/10.1007/bf00028772.

Sousa, A.J.S., Silva, C.F.B., Sousa, J.S., Monteiro, J.E., Freire, J.E.C., Sousa, B.L., Lobo, M. D.P., Monteiro-Moreira, A.C.O., Grangeiro, T.B., 2019. A thermostable chitinase from the antagonistic *Chromobacterium violaceum* that inhibits the development of phytopathogenic fungi. Enzym. Microb. Technol. 126, 50–61. https://doi.org/10.1016/j.enzmictec.2019.03.009.

Taira, T., Mahoe, Y., Kawamoto, N., Onaga, S., Iwasaki, H., Ohnuma, T., Fukamizo, T., 2011. Cloning and characterization of a small family 19 chitinase from moss (*Bryum coronatum*). Glycobiology 21, 644–654. https://doi.org/10.1093/glycob/cwq212.

Taira, T., Ohnuma, T., Yamagami, T., Aso, Y., Ishiguro, M., Ishihara, M., 2002. Antifungal activity of rye (*Secale cereale*) seed chitinases: the different binding manner of class I and class II chitinases to the fungal cell walls. Biosci. Biotechnol. Biochem. 66, 970–977. https://doi.org/10.1271/bbb.66.970.

Terwisscha van Scheltinga, A.C., Armand, S., Kalk, K.H., Isogai, A., Henrissat, B., Dijkstra, B.W., 1995. Stereochemistry of chitin hydrolysis by a plant chitinase/lysozyme and X-ray structure of a complex with allosamidin: evidence for substrate assisted catalysis. Biochemistry 34, 15619–15623.

Trott, O., Olson, A.J., 2010. AutoDock Vina: improving the speed and accuracy of docking with a new scoring function, efficient optimization, and multithreading. J. Comput. Chem. 31, 455–461. https://doi.org/10.1002/jcc.21334.

Truong, N.-H., Park, S.-M., Nishizawa, Y., Watanabe, T., Sasaki, T., Itoh, Y., 2003. Structure, heterologous expression, and properties of rice (*Oryza sativa* L.) family 19 chitinases. Biosci. Biotechnol. Biochem. 67, 1063–1070. https://doi.org/10.1271/bbb.67.1063.

Tyler, L., Bragg, J.N., Wu, J., Yang, X., Tuskan, G.A., Vogel, J.P., 2010. Annotation and comparative analysis of the glycoside hydrolase genes in *Brachypodium distachyon*. BMC Genom. 11, 600. https://doi.org/10.1186/1471-2164-11-600.

van Loon, L.C., Rep, M., Pieterse, C.M.J., 2006. Significance of inducible defense-related proteins in infected plants. Annu. Rev. Phytopathol. 44, 135–162. https://doi.org/10.1146/annurev.phyto.44.070505.143425.

Volk, H., Marton, K., Flajšman, M., Radišek, S., Tian, H., Hein, I., Podlipnik, Č., Thomma, B.P.H.J., Košmelj, K., Javornik, B., Berne, S., 2019. Chitin-binding protein of *Verticillium nonalfalfae* disguises fungus from plant chitinases and suppresses chitin-triggered host immunity. Mol. Plant Microbe Interact. 32, 1378–1390. https://doi.org/10.1094/MPMI-03-19-0079-R.

Warner, S.A.J., 1996. Genomic DNA isolation and lambda library construction. In: Foster, G.D., Twell, D. (Eds.), Plant Gene Isolation: Principles and Practice. John Wiley & Sons, West Sussex, pp. 51–73.

Whelan, S., Goldman, N., 2001. A general empirical model of protein evolution derived from multiple protein families using a maximum-likelihood approach. Mol. Biol. Evol. 18, 691–699. https://doi.org/10.1093/oxfordjournals.molbev.a003851.

Zhang, D., Hrmova, M., Wan, C.-H., Wu, C., Balzen, J., Cai, W., Wang, J., Densmore, L.D., Fincher, G.B., Zhang, H., Haigler, C.H., 2004. Members of a new group of chitinase-like genes are expressed preferentially in cotton cells with secondary walls. Plant Mol. Biol. 54, 353–372. https://doi.org/10.1023/B:PLAN.0000036369.55253.dd.

Zhong, R., Kays, S.J., Schroeder, B.P., Ye, Z.-H., 2002. Mutation of a chitinase-like gene causes ectopic deposition of lignin, aberrant cell shapes, and overproduction of ethylene. Plant Cell 14, 165–179. https://doi.org/10.1105/tpc.010278.